


Dark state semilocalization of quantum emitters in a cavityT. Botzung,^{1,2,3} D. Hagenmüller,¹ S. Schütz,^{1,4} J. Dubail,^{5,1} G. Pupillo,^{1,6,*} and J. Schachenmayer^{1,4,†}¹*Université de Strasbourg and CNRS, ISIS (UMR 7006) and icFRC, 67000 Strasbourg, France*²*Institute for Quantum Information, RWTH Aachen University, D-52056 Aachen, Germany*³*Peter Grünberg Institute, Theoretical Nanoelectronics, Forschungszentrum Jülich, D-52425 Jülich, Germany*⁴*IPCMS (UMR 7504), CNRS, 67000 Strasbourg, France*⁵*Université de Lorraine, CNRS, LPCT, F-54000 Nancy, France*⁶*Institut Universitaire de France (IUF), 75000 Paris, France* (Received 23 March 2020; revised 5 October 2020; accepted 6 October 2020; published 28 October 2020)

We study a disordered ensemble of quantum emitters collectively coupled to a lossless cavity mode. The latter is found to modify the localization properties of the “dark” eigenstates, which exhibit a character of being localized on multiple noncontiguous sites. We denote such states as semilocalized and characterize them by means of standard localization measures. We show that those states can very efficiently contribute to coherent energy transport. Our paper underlines the important role of dark states in systems with strong light-matter coupling.

DOI: [10.1103/PhysRevB.102.144202](https://doi.org/10.1103/PhysRevB.102.144202)**I. INTRODUCTION**

When quantum emitters and a cavity mode coherently exchange energy at a rate faster than their decay, hybrid light-matter states play an important role [1–3]. Such polaritonic states are superpositions composed of “bright” emitter modes and cavity photons, while numerous remaining emitter states have no photon contribution, i.e., remain “dark.” Collective strong light-matter coupling has been intensively pursued in atomic [4–6] and condensed-matter physics [7–12]. Very recently, strong collective coupling has been explored as a tool to engineer fundamental properties of matter, e.g., the critical temperature of superconductors [13,14] or chemical reaction rates [15–22]. Much interest is currently raised by the possibility of modifying energy [23–30] and charge [30–33] transport.

For transport, disorder plays a crucial role. It is well studied that coherent transport is inhibited due to Anderson localization (AL) [34]. Here, an arbitrarily small disorder can lead to a localization of eigenstates in 1D and 2D [34,35], while in 3D a metal–insulator transition driven by the disorder strength occurs [34,36]. Here, we study the fate of this phenomenon in a cavity. It is known that polaritonic states are largely unaffected by disorder [37] and the impact of disorder on polariton physics for laser-driven setups has been extensively explored [38–42]. While for transport problems it is known that polariton states can lead to a considerable enhancement of energy transmission [24–30], the localization and transport properties of dark states have remained largely unexplored. It is clear that disorder leads to a mixing of the bright with the dark states [43], which strongly alters the usual description of light-matter coupling. Addressing these issues is for example

important for applications of radiative energy transmission in mesoscopic systems.

In this paper, we investigate a simple model for AL and coherent energy transport with N emitters collectively coupled to a cavity mode [Fig. 1(a)]. We focus on the impact of the cavity coupling on localized eigenstates, i.e., for a disorder strength much larger than the excitation hopping rate. We focus on dark states and find that they exhibit several surprising features: for any strength of light-matter interactions, they acquire a squared amplitude $\sim 1/N$, on average, for arbitrary distances. While their photon weight vanishes, they can remain localized according to standard localization measures, such as the inverse participation ratio (IPR) in the thermodynamic limit. However, we find that localization is distributed over multiple sites, which can be arbitrarily distant from one another. For large cavity coupling, they can be considered as hybridizations of a few localized states of the uncoupled system, and their energy lies in between those of the bare states. This results in semi-Poissonian statistics of energy-level spacings, which neither corresponds to a fully localized nor extended phase. We find that semilocalized states are responsible for diffusivelike dynamics, which is at odds with their localized nature. On average, the exponential decay of an excitation current with N for AL can be turned into an algebraic decay $\sim 1/N$, and can thus dominate over the $\sim 1/N^2$ contribution expected from polariton states. The nonlocal nature of the cavity coupling makes these effects independent of the dimensionality.

Our results are directly relevant for setups with condensed matter interacting with confined electromagnetic fields (both close to a vacuum state [13–33] or laser-driven [44–55]), in particular, for recent coherent transport setups [56,57]. Furthermore, in the past years, localization has been extensively experimentally explored with controlled disorder in cold atom systems [58–61], even in interacting many-body regimes (many-body localization) [62]. Specifically,

*pupillo@unistra.fr

†schachenmayer@unistra.fr

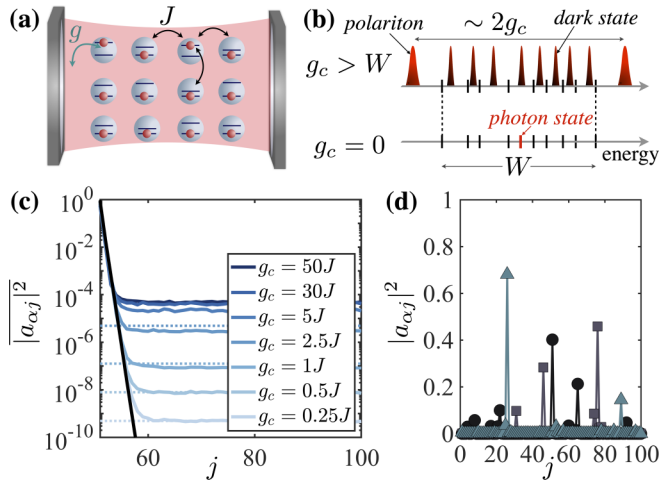


FIG. 1. (a) An excitation can hop with rate J on a disordered 3D lattice with N sites. Local transitions are coupled to a cavity with collective strength $g_c \equiv g\sqrt{N}$. (b) For $g_c = J = 0$, the N bare levels are randomly distributed in $[-W/2, W/2]$. For $g_c > W$, the spectrum contains two polariton eigenstates (splitting $\sim 2g_c$) and $N - 1$ dark states lying in between the bare levels. (c) Modification of the disorder-averaged weights of a dark eigenstate localized in the middle of a chain (1D for convenience) with $N = 100$, 2000 realizations, $W = 25J$. In addition to exponential localization at short distances (black line, $g_c = 0$), a constant tail appears for $g_c > 0$ (dashed lines: perturbative results). (d) Single disorder realization: Three dark eigenstates are shown for $g_c = 50J$ and $W = 25J$.

experiments using Dicke model realizations based on Raman-dressed hyperfine ground states of intracavity trapped atoms, as recently achieved [63,64], could be used to study the semilocalized physics described here. We propose a specific cold atom implementation of our model in Appendix E. Models of emitters interacting with a single cavity mode are also formally similar to central spin models [65,66] that have been very successful in modeling hyperfine interactions of quantum dots surrounded by a bath of nuclear spins [67–69]; the effects of disorder in central spin models have been investigated recently in Refs. [70,71] in connection with many-body localization.

The remainder of the paper is organized as follows. In Sec. II, we introduce the model under consideration. In Sec. III, we discuss the physics of the model in various regimes and show that localized eigenstates acquire an average probability amplitude for arbitrary distances for strong enough light-matter couplings. This semilocalization behavior is characterized by standard localization measures such as the return probability, the IPR (Sec. III A), and the level statistics (Sec. III B). In Sec. IV, we explore the model dynamics by computing the excitation current flowing through the system and the time dependence of the mean-square displacement. We provide a conclusion in Sec. V.

II. MODEL

We start by considering a 3D cubic lattice of N two-level systems embedded in a cavity. The Hamiltonian ($\hbar \equiv 1$) is

$$\hat{H} = \hat{H}_0 + \hat{H}_1, \text{ with}$$

$$\hat{H}_0 = \omega_c \hat{a}^\dagger \hat{a} + \sum_i (\omega_e + w_i) \hat{\sigma}_i^+ \hat{\sigma}_i^- - J \sum_{\langle i,j \rangle} \hat{\sigma}_i^+ \hat{\sigma}_j^- \quad (1)$$

and

$$\hat{H}_1 = g \sum_i (\hat{a} \hat{\sigma}_i^+ + \hat{a}^\dagger \hat{\sigma}_i^-). \quad (2)$$

We restrict our discussion to a Hilbert space with a single excitation, i.e., $\sum_i \hat{\sigma}_i^+ \hat{\sigma}_i^- + \hat{a}^\dagger \hat{a} = \mathbb{1}$. Then, there are $N + 1$ basis states, $|i, 0\rangle$, $|G, 1\rangle$, denoting states with an excitation on site i , or in the cavity, respectively. Also considering the state without excitation, $|G, 0\rangle$, the spin lowering and photon annihilation operators are defined as $\hat{\sigma}_i^- = |G, 0\rangle \langle i, 0|$ and $\hat{a} = |G, 0\rangle \langle G, 1|$. In all numerical calculations, we consider the cavity mode (frequency ω_c) in resonance with the average emitter transition (ω_e), i.e., $\delta \equiv \omega_e - \omega_c = 0$. The third term in \hat{H}_0 governs hopping (rate J) between nearest-neighbor sites, indicated by the notation $\langle i, j \rangle$. Assuming periodic boundaries, this term is diagonalized by introducing the operators $\hat{b}_q = \sum_i \exp(-iq \cdot i) \hat{\sigma}_i^- / \sqrt{N}$. The second term contains on-site disorder, with w_i random variables uniformly distributed in $[-W/2, W/2]$. The other term, H_1 , describes the Tavis-Cummings emitter-cavity coupling [1] with local strengths g . This term can be written in the form

$$H_1 = g_c (\hat{a} \hat{b}_0^\dagger + \hat{a}^\dagger \hat{b}_0) \quad (3)$$

with the collective strength $g_c = g\sqrt{N}$, and couples the symmetric bright mode $\hat{b}_{q=0}$ to cavity photons. Importantly, g decreases with the cavity-mode volume V as $g \sim 1/\sqrt{V}$ [72] and g_c thus remains independent of N for fixed density N/V .

III. SEMILOCALIZATION

A. Semilocalized eigenstates

In the absence of disorder ($W = 0$), \hat{H} has two polariton eigenstates $|\psi_\pm\rangle = (\hat{b}_{q=0}^\dagger \pm \hat{a}^\dagger) / \sqrt{2} |G, 0\rangle$ with energies $E_\pm = \pm g_c$, as well as $N - 1$ uncoupled dark states $|\psi_{\alpha \neq \pm}\rangle = \hat{b}_{q \neq 0}^\dagger |G, 0\rangle$ with vanishing photon weight, $\langle G, 1 | \psi_{\alpha \neq \pm} \rangle = 0$. It is obvious that finite disorder ($W \neq 0$) leads to a coupling between the bright and the dark states since \hat{H}_1 is nondiagonal in quasimomentum space. The dark eigenstates therefore acquire a small photonic weight $|\langle G, 1 | \psi_{\alpha \neq \pm} \rangle|^2 \sim 1/N$ (see Appendix A), and become grey. In the following, we are interested in the modification of the emitter part of the system and define the normalized emitter amplitudes as $a_{\alpha j} \equiv \langle j, 0 | \psi_\alpha \rangle / \sqrt{N_\alpha}$ with $N_\alpha = 1 - |\langle G, 1 | \psi_\alpha \rangle|^2$.

For $g_c = 0$, \hat{H} corresponds to a usual AL model, displaying a W -dependent mobility edge that determines a metal-insulator transition at $W_c \simeq 16.5J$ (for energy states in the middle of the band) [73–76]. While for $W \ll W_c$ the eigenstates $|\psi_\alpha\rangle$ resemble extended Bloch states, they are localized around given sites for $W > W_c$, e.g., $|a_{\alpha j}|^2 \propto e^{-|i-j|/\xi}$ for a state localized on site i , with ξ a W/J -dependent localization length. In the following, we investigate the case $g_c, W \neq 0$, and focus on spectral and transport properties of the Anderson insulator for strong collective light-matter couplings $g_c > W > W_c$.

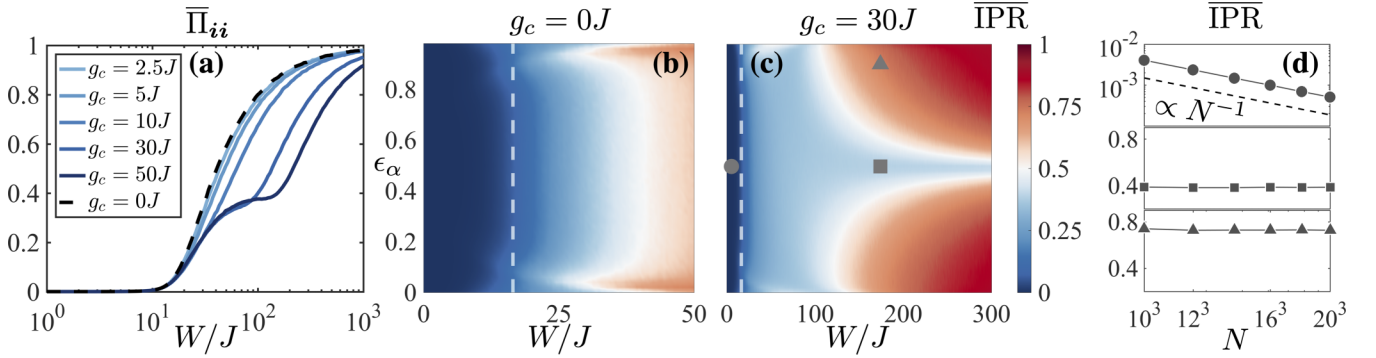


FIG. 2. (a) Disorder-averaged return probability $\overline{\Pi}_{ii}$ as a function of W/J (for the central site i of a $N = 15^3$ cube, mean emitter splitting on resonance with cavity, $\delta = 0$). For strong couplings $g_c > W > W_c$, a plateau ($\overline{\Pi}_{ii} \simeq 0.4$) indicates a semilocalized regime. (b)–(c) Disorder-averaged inverse participation ratio $\overline{\text{IPR}}(\epsilon_\alpha)$ as a function of W/J and the renormalized dark state energy ϵ_α (bins of widths 0.02, ~ 100 realizations, white dashed line: $W = W_c$). (b) $g_c = 0$ (no cavity); (c) $g_c = 30J$ (larger W/J scale), showing an extended area with $\overline{\text{IPR}}(\epsilon_\alpha) \simeq 0.4$. (d) Finite-size scaling of $\overline{\text{IPR}}(\epsilon_\alpha)$ for the parameters corresponding to the symbols in (c). Circle ($W = 5J$, $\epsilon_\alpha = 0.5$); square ($W = 175J$, $\epsilon_\alpha = 0.5$); triangle ($W = 175J$, $\epsilon_\alpha = 0.9$).

The modification of AL in a cavity can be understood by first considering the eigenstates of \hat{H} for $J = 0$, in which case the spatial dimensionality becomes irrelevant. In second-order perturbation theory (see Appendix A), a trivially localized eigenstate on site i , $|\mathbf{i}, 0\rangle$, for $g_c = 0$ acquires an amplitude on site $j \neq i$ via the cavity,

$$b_{i \neq j} = \frac{g^2}{(w_i - w_j)(w_i + \delta)}, \quad (4)$$

valid for configurations with $g^2 \ll |(w_i - w_j)(w_i + \delta)|$. A lower bound for the squared amplitude of perturbed localized states is thus $|b_{i \neq j}|^2 \geq 4g_c^4/(N^2W^4)$, setting $\delta = 0$. In Appendix A, we use perturbation theory to derive that the averaged value over disorder realizations is

$$\overline{|b_{i \neq j}|^2} = \frac{4g_c^4[4 - 2\log(4)]}{NW^4} \quad (5)$$

for large N . In Fig. 1(c), we show numerically that also for finite $J \ll W$ the weights of an eigenstate localized in the center of a 1D chain, logarithmically averaged over disorder realizations, maintains an exponentially localized profile at short distances, followed by a constant tail rising with g_c . The tails are consistent with our perturbative result for small g (dashed lines) and saturate for strong couplings $g_c > W > J$. Note that a similar behavior was reported for dissipative couplings to a common reservoir [77,78].

For strong coupling ($g_c > W > J$), two polaritonic states $|\psi_\pm\rangle$ with $|\langle G, 1|\psi_\pm\rangle|^2 \approx 0.5$ and separated by a splitting $\sim 2g_c$ (only slightly modified by disorder) emerge from the band of width W . We find that the energies of the $N - 1$ dark states lie in between the N bare ($g_c = 0$) levels [Fig. 1(b)], which can be seen as a simple consequence of the arrowhead matrix shape of the single-excitation Hamiltonian for $J = 0$, as we detail in Appendix B. The strong cavity coupling leads to a hybridization between bare levels, close in energy, but not necessarily in real space. For a single disorder realization, the dark states appear strongly localized at multiple sites [Fig. 1(d)]. We term this behavior *semilocalization*.

Information about the spatial localization of dark eigenstates with energy E_α is given by the IPR:

$$\text{IPR}(E_\alpha) = \sum_{i=1}^N |a_{\alpha i}|^4. \quad (6)$$

A finite, size-independent IPR indicates a localized eigenstate, while an IPR scaling as $1/N \rightarrow 0$ indicates an extended one. Initializing the system in the state $|\mathbf{i}, 0\rangle$, the infinite-time-averaged probability to find an excitation at site j is

$$\Pi_{ij} = \lim_{T \rightarrow \infty} \frac{1}{T} \int_0^T dt P_{ij}(t), \quad (7)$$

with $P_{ij}(t) \equiv |\langle j, 0|\phi(t)\rangle|^2$ and $|\phi(t)\rangle = e^{-i\hat{H}t} |\mathbf{i}, 0\rangle$. The IPR is connected to the return probability Π_{ii} by $\sum_i \Pi_{ii} = \sum_\alpha \text{IPR}(E_\alpha) \mathcal{N}_\alpha^2$. The $\text{IPR}(E_\alpha)$ can thus be interpreted as the contribution of a given eigenstate to $\sum_i \Pi_{ii}$.

In Fig. 2(a), we compute numerically the disorder average of Π_{ii} , $\overline{\Pi}_{ii}$, for the central site of a cubic lattice ($N = 15^3$). For $g_c = 0$ (dashed line), $\overline{\Pi}_{ii}$ increases from 0 (extended phase) to 1 (localized phase) upon increasing the disorder strength W/J . Remarkably, we find that $\overline{\Pi}_{ii}$ exhibits a plateau $\simeq 0.4$ for $g_c > W > J$, which persists up to large disorder strengths ($W \sim 100J$ for $g_c = 50J$).

The disorder-averaged IPR, $\overline{\text{IPR}}(E_\alpha)$, is shown in Figs. 2(b) and 2(c) as a function of W/J for the AL model ($g_c = 0$) and for $g_c = 30J$. As we only focus on dark states (in the band of width W), we use a dimensionless, renormalized energy scale $\epsilon_\alpha = (E_\alpha - W/2)/W$ with $\epsilon_\alpha \in [0, 1]$. For each disorder realization, we bin different levels into groups with equal energy width and then average over realizations in each bin. Figure 2(b) shows the emergence of localized states upon increasing W/J , starting from the edges of the spectrum. A strong cavity coupling [Fig. 2(c)] leads to *three* distinct regimes: (i) a delocalized region [$\overline{\text{IPR}}(\epsilon_\alpha) \sim 0$ for $W \lesssim W_c$], (ii) a fully localized region [$\overline{\text{IPR}}(\epsilon_\alpha) \sim 1$ for $W > g_c$], and (iii) an extended area with $\overline{\text{IPR}}(\epsilon_\alpha) \sim 0.4$ where the dark states feature semilocalized characteristics consistent with the return probability and the results shown in Fig. 1(c). The persistence of semilocalized states in the vicinity of $\epsilon_\alpha = 0.5$

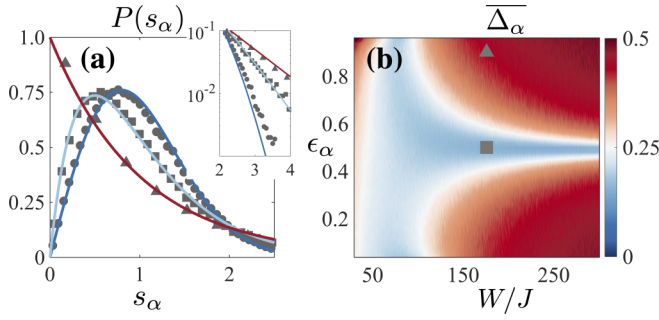


FIG. 3. (a) Comparison of numerically computed distributions $P(s_\alpha)$ [symbols, parameters as in 2(c)] with analytical formulas (lines, see text). Wigner-Dyson distribution (dark blue), Poissonian distribution (red), semi-Poissonian distribution (light blue). Inset: Tails of the distributions on a logarithmic scale. (b) Numerically computed “dark state deviations” $\overline{\Delta}_\alpha$ (see text) as a function of W/J for $g_c = 30J$.

($\delta = 0$) can be understood from the failure of perturbation theory, even for $W \gg g_c$. The energy separation between the two levels (i_0, j_0) closest to $\epsilon_\alpha = 0.5$ is $(w_{i_0} - w_{j_0}) \sim W/N$. For them, the perturbation condition $g_c^2 \ll W(w_{i_0/j_0} + \delta)$ is violated for all W considered in Fig. 2(c), as they hybridize via the cavity.

In Fig. 2(d), we analyze the finite size scaling of $\overline{\text{IPR}}(\epsilon_\alpha)$ in the three regions [for parameters corresponding to the symbols in Fig. 2(c)]. We observe that the IPR of semilocalized states does not scale with the system size. These states exhibit the same behavior as in the fully localized region, only with a reduced value, which is consistent with states localized on multiple sites. In contrast, $\overline{\text{IPR}}(\epsilon_\alpha) \propto 1/N$ for extended states.

B. Level statistics

Localization properties of eigenstates are also characterized by their level statistics [76]. Here, we numerically analyze the probability distribution function $P(s_\alpha)$ for spacings between adjacent eigenenergies, $s_\alpha = \epsilon_{\alpha+1} - \epsilon_\alpha$. In Fig. 3(a), we plot $P(s_\alpha)$ for eigenstates corresponding to the symbols in Fig. 2(c). While in the delocalized region ($W \lesssim W_c$) $P(s_\alpha) = \frac{\pi}{2} s_\alpha \exp(-\frac{\pi}{4} s_\alpha^2)$ follows a Wigner-Dyson distribution, the fully localized phase is characterized by a Poissonian, $P(s_\alpha) = \exp(-s_\alpha)$ [79]. Interestingly, we observe that the semilocalized region features semi-Poissonian [80] statistics, $P(s_\alpha) = 4s_\alpha \exp(-2s_\alpha)$. We have checked that this behavior appears in the entire semilocalized region and is independent of N . The semi-Poissonian form can be simply understood for $J = 0$. Then, bare ($g_c = 0$) levels follow a Poisson distribution. Since for strong coupling ($g_c > W$), dark states lie in between the bare levels, we can model the dark state distribution as

$$P(s_\alpha) = \int dx dy \delta\left(s_\alpha - \frac{x+y}{2}\right) e^{-x} e^{-y} = 4s_\alpha e^{-2s_\alpha},$$

where we assumed the hybridized states equidistant from the two closest bare levels. To check the validity of this assumption for $J \neq 0$, we analyze numerically the disorder-averaged

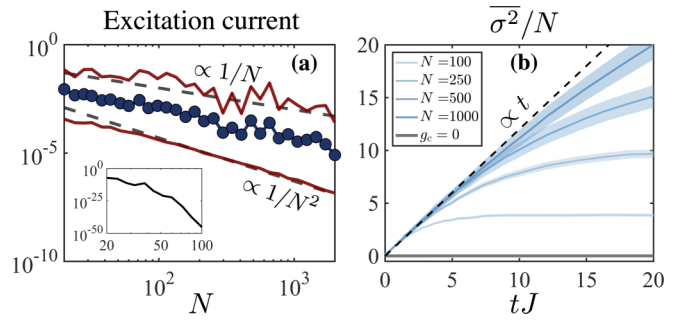


FIG. 4. (a) Excitation currents through a 1D chain as function of N (strong coupling, $g_c = 30J$, $W = 10J$, $\gamma = 0.05J$, currents averaged over finite times $1000 \leq tJ \leq 2000$, see text). Shown are the mean (\bar{I} , blue circles) and maximum/minimum currents ($I_{\max/\min}$, red lines) of 100 disorder realizations. Dashed lines are guides to the eye for $1/N$ and $1/N^2$. Inset: $\bar{I} \propto e^{-N}$ for $g_c = 0$. (b) Disorder-averaged mean squared displacement $\overline{\sigma^2}/N$ (1D, $g_c = 50J$, $W = 30J$, 200 realizations, shaded area: standard error of the mean, see text). While absence of diffusion is found for $g_c = 0$ ($\overline{\sigma^2}/N \simeq 0$, grey line, expected for 1D Anderson localization), diffusive-like dynamics, $\overline{\sigma^2} \propto t$, occurs for $g_c \gg W$.

deviation,

$$\overline{\Delta}_\alpha = N \left(E_\alpha - \frac{w_i + w_{i+1}}{2} \right), \quad (8)$$

in Fig. 3(b), with w_i and w_{i+1} the closest bare levels immediately below and above E_α . While in the localized phase (triangle) the eigenenergies are found to be very close to the bare levels, they are much closer to $(w_i + w_{i+1})/2$ in the semilocalized region (square), confirming our simple argument above.

IV. DARK STATE TRANSPORT

Finally, we discuss the role of semilocalized states on transport and diffusion. We have seen that localization properties in the semilocalized regime can be well understood for $J = 0$. In this case, the dimensionality of the problem becomes irrelevant (see Appendix D). Therefore, for simplicity, we here focus on transport in 1D for a chain with sites $i = 1, \dots, N$.

We expect that, generally, the semilocalized dark state can very efficiently contribute to transport. Since the polaritonic states feature homogeneous amplitudes $a_{\pm,i} \sim 1/\sqrt{N}$ throughout the system, they contribute to the infinite-time averaged transmission probability, $\Pi_{1N} \sim \sum_\alpha |a_{\alpha 1}|^2 |a_{\alpha N}|^2$, with a term $\sim 1/N^2$. In contrast, semilocalized dark states contribute with terms $\sim 1/N$ when averaging over disorder realizations. This stems from the fact that the probability for an excitation to leave a site i , $1 - \overline{\Pi}_{ii} \sim 0.6$ is independent of N . Therefore the infinite-time averaged transmission probability to any other site is $\sim (1 - \overline{\Pi}_{ii})/(N - 1) \sim 0.6/(N - 1)$, which explains the $\overline{\Pi}_{1N} \sim 1/N$ contribution.

For a realistic transport scenario, in Fig. 4(a), we analyze the excitation current flowing through a chain, as a function of N , while keeping the emitter density constant. To compute such currents, we imagine the 1D chain to be connected to two Markovian baths at the two ends. We consider the system to be initially in the state $|G, 0\rangle$, turn the bath coupling on, and

simulate the time-evolution. The Lindblad master equation governing the dynamics is

$$\frac{d\hat{\rho}}{dt} = -i[\hat{H}, \hat{\rho}] + \sum_{\eta} \hat{\mathcal{L}}_{\eta}(\hat{\rho}), \quad (9)$$

with $\hat{\rho}$ the density matrix and two dissipative Lindblad processes adding/removing excitations on the first and last site. Here,

$$\hat{\mathcal{L}}_{\eta}(\hat{\rho}) = -\{\hat{L}_{\eta}^{\dagger}\hat{L}_{\eta}, \hat{\rho}\} + 2\hat{L}_{\eta}\hat{\rho}\hat{L}_{\eta}^{\dagger}, \quad (10)$$

with $\hat{L}_{\text{in}} = \sqrt{\gamma/2}\hat{\sigma}_1^{+}$ and $\hat{L}_{\text{out}} = \sqrt{\gamma/2}\hat{\sigma}_N^{-}$ with γ a pumping rate. The excitation current can be computed as $I \equiv \text{Tr}[\hat{\sigma}_N^{+}\hat{\sigma}_N^{-}\hat{\rho}]$ [25]. In contrast to previous simulations of such scenarios (e.g., in Ref. [25]), there are no additional dissipative decay channels in our coherent transport model. We therefore find that the dynamics of I exhibits persistent small oscillations up to long times. We therefore average over the timescale $1000 \leq tJ \leq 2000$. At those late times, we still observe a very slow decrease of the current with time for the smaller system sizes. For $N > 1000$, we don't find any significant evolution. The data in Fig. 4 is additionally averaged over 100 disorder realizations. For $g_c = 0$, we always find an exponentially suppressed current, $\bar{I} \sim \exp(-N)$, while for strong coupling ($g_c = 30J$) the mean current decays slower, closer to a $\bar{I} \sim 1/N$ scaling. Additionally, we also plot maximum (minimum) currents I_{max} (I_{min}) of the realizations. For large N , I_{min} decreases as $\sim 1/N^2$ and exhibits only small fluctuations. We interpret this as an unlucky disorder realization prohibiting efficient dark-state transport, requiring the energy to flow through polaritonic states [25]. We note that it is not clear whether the $1/N$ scaling of the finite time currents from Fig. 4(a) can be related to the $\sim 1/N$ contribution in the infinite time averaged quantity $\bar{\Pi}_{1N}$ [81].

In Fig. 4(b), we analyze the diffusion properties in the 1D chain, after initializing the system in the state $|\phi(t=0)\rangle = |N/2, 0\rangle$. We show the time evolution of the disorder-averaged mean-squared displacement $\overline{\sigma^2} = \sum_j |i-j|^2 \bar{P}_{ij}(t)$. For $g_c = 0$ and $W = 30J$, eigenstates are fully localized and diffusion is suppressed, $\overline{\sigma^2} \sim \text{cst}$, while a diffusivelike behavior $\lim_{N \rightarrow \infty} \overline{\sigma^2} \propto t$ occurs in the strong coupling case ($g_c = 50J$) up to finite size effects. Second order perturbation theory (Schrieffer-Wolff transformation [82]) leads to an effective *correlated* hopping model (see Appendix C for a detailed derivation), with on-site energy dependent amplitude, which differs from other known disordered models, e.g., with power-law hopping [83–87]. Diffusivelike behavior can be qualitatively understood for $J = 0$: the transition probability $P_{ij}(t)$ is then not correlated with distance $|i-j|$, so

$$\begin{aligned} \overline{\sigma^2} &= \sum_j |i-j|^2 \sum_{k \neq i} \frac{\bar{P}_{ik}(t)}{N} \\ &\simeq \frac{1 - \bar{P}_{ii}(t)}{N} \sum_j |i-j|^2 \propto N^2 [1 - \bar{P}_{ii}(t)]. \end{aligned} \quad (11)$$

The escape probability can be estimated to increase linear in time, $1 - P_{ii}(t) \propto t/N$, with Fermi's golden rule for large N (as shown in Appendix C). We note that this behavior does not correspond, strictly speaking, to a diffusive dynamics since

the increase of the mean-squared displacement is nonlocal and stems from the evenly distributed growth of the probability amplitudes $a_{\alpha j}$ over the whole chain [see Fig. 1(d)].

V. CONCLUSION

We have shown that AL can be strongly modified by coupling the disordered ensemble to a cavity. This is manifested by the emergence of dark states localized on multiple sites with energy spacings following semi-Poissonian statistics. We denote such states as *semilocalized*. We find that typical localization quantifiers such as the IPR exhibit properties common to ordinarily localized states (constant scaling with system size) but at values below one, $\overline{\text{IPR}}(\epsilon_{\alpha}) \sim 0.4$. Additionally, in this semilocalized regime, the level-spacing statistics exhibits a semi-Poissonian behavior, which neither corresponds to ordinary localized states (Poissonian distribution) nor extended states (Wigner-Dyson distribution). We further analyzed the contribution of semilocalized states to transport and found that they are responsible for a diffusivelike behavior and an algebraic decay of energy transmission for strong light-matter couplings. It is an interesting prospect to investigate how dissipation [77] affects the transport properties of such states.

ACKNOWLEDGMENTS

We are grateful to Denis Basko, Claudiu Genes, Nikolay Prokof'ev, Antonello Scardicchio, Giuseppe Luca Celardo, Francesco Mattiotti, and Fausto Borgonovi for stimulating discussions. This work was supported by the ANR - ERA-NET QuantERA—Projet RouTe (ANR-18-QUAN-0005-01), and LabEx NIE (Nanostructures in Interaction with their Environment) under Contract No. ANR-11-LABX0058 NIE with funding managed by the French National Research Agency as part of the Investments for the Future program (Program No. ANR-10-IDEX-0002-02), and IdEx Unistra project STEMQuS. G.P. acknowledges support from the Institut Universitaire de France (IUF) and the University of Strasbourg Institute of Advanced Studies (USIAS). Research was carried out using computational resources of the Centre de calcul de l'Université de Strasbourg.

APPENDICES

In the following Appendices, we provide further details on analytical calculations: We discuss our perturbation theory (Appendix A), arrowhead matrix calculations (Appendix B), and the Schrieffer-Wolff transformation for estimating diffusion with Fermi's golden rule (Appendix C). We provide results for the return probability also in 1D systems (Appendix D). Lastly, we describe a scheme how one could implement our model in recent cold atom experiments (Appendix E).

APPENDIX A: PERTURBATION THEORY

We start from the Hamiltonian \hat{H}_0 without hopping ($J = 0$), and treat the light-matter coupling contribution H_1 as a perturbation. To second order, the eigenstates

$$|i, 0\rangle^{(2)} = |i, 0\rangle + \frac{g}{w_i + \delta} |G, 1\rangle + \sum_{j \neq i} b_{i \neq j} |j, 0\rangle \quad (A1)$$

acquire a finite amplitude on site $j \neq i$ via the cavity:

$$b_{i \neq j} \equiv \langle j, 0 | i, 0 \rangle^{(2)} = \frac{g^2}{(w_i - w_j)(w_i + \delta)}. \quad (\text{A2})$$

Note that (taking $\delta = 0$) the individual perturbative state amplitudes in Eq. (A1) are valid for $g^2 \ll |w_i(w_i - w_j)|$, which is satisfied in the thermodynamic limit $N \rightarrow \infty$ for a fixed g_c , as long as w_i is not too close to the middle of the distribution $w_i = 0$ and for w_i and w_j not accidentally in close resonance.

An analytic expression of the constant tail [Fig. 1(c) of the main text] can be derived in the perturbative regime by computing the disorder average of the squared amplitudes $b_{i \neq j}$ in the limit $N \rightarrow \infty$. For $\delta = 0$, we obtain

$$\begin{aligned} \overline{|b_{i \neq j}|^2} &= \frac{1}{N} \sum_i \sum_{j \neq i} |b_{i \neq j}|^2 \\ &= \frac{g^4}{N} \int_{-W/2}^{W/2} d\omega \frac{\rho(\omega)}{\omega^2} \int_{-W/2}^{W/2} d\omega' \frac{\rho(\omega')}{(\omega - \omega')^2}, \end{aligned} \quad (\text{A3})$$

with the uniform density of states $\rho(\omega) = N/W$. Because of the divergence for $\omega = \omega'$ occurring in the second integral, we compute the Hadamard finite part of the latter:

$$\begin{aligned} \mathcal{H} \int_{-W/2}^{W/2} d\omega' \frac{\rho(\omega')}{(\omega - \omega')^2} &= \lim_{\epsilon \rightarrow 0} \left[\int_{-W/2}^{\omega - \epsilon} d\omega' \frac{\rho(\omega')}{(\omega - \omega')^2} \right. \\ &\quad \left. + \int_{\omega + \epsilon}^{W/2} d\omega' \frac{\rho(\omega')}{(\omega - \omega')^2} - \frac{2}{\epsilon} \right] \\ &= \frac{W}{\omega^2 - (W/2)^2}. \end{aligned} \quad (\text{A4})$$

Using this result in Eq. (A3) and considering again the finite part (removing the divergences at $\omega = 0$ and $\omega = \pm W/2$) of the remaining integral, we obtain the result given in the main text:

$$\overline{|b_{i \neq j}|^2} = \frac{4g_c^4 [4 - 2 \log(4)]}{NW^4} \quad (g_c = g\sqrt{N}). \quad (\text{A5})$$

This prediction agrees very well with numerically exact simulations (see main text) for $g_c \ll W$, indicating that occasional resonances and the divergence at $\omega = 0$ do not play an important role for the averaged tails of the eigenstates.

APPENDIX B: ARROWHEAD HAMILTONIAN

In the single-excitation subspace, the Hamiltonian \hat{H} without hopping ($J = 0$) takes the form of an arrowhead matrix in the basis $\{|i, 0\rangle, |G, 1\rangle\}$

$$\hat{H} = \left(\begin{array}{cccc|cc} w_1 & 0 & & \dots & 0 & g \\ 0 & w_2 & 0 & & & \\ & 0 & \ddots & \ddots & & \vdots \\ \vdots & & \ddots & & 0 & \vdots \\ & & & & 0 & w_{N-1} & 0 \\ 0 & \dots & & & 0 & w_N & g \\ \hline g & & & \dots & & g & 0 \end{array} \right). \quad (\text{B1})$$

A direct property of this arrowhead form is that after sorting the bare energies w_j in increasing order, i.e., $w_1 \leq w_2 \leq \dots$

$\leq w_N$, the eigenvalues of H are interlaced with those bare energies [88]:

$$\epsilon_- \leq w_1 \leq \epsilon_1 \leq w_2 \leq \dots \leq w_{N-1} \leq \epsilon_{N-1} \leq w_N \leq \epsilon_+. \quad (\text{B2})$$

In the strong coupling case, the two eigenvalues ϵ_{\pm} at the edges of the spectrum correspond to the polariton-state frequencies $\sim \pm g_c$, while the remaining ones $\epsilon_1, \epsilon_2, \dots, \epsilon_{N-1}$ correspond to the $N - 1$ dark state frequencies denoted as ϵ_α in the main text. The $N + 1$ eigenstates satisfying $\hat{H}\psi_\alpha = \epsilon_\alpha\psi_\alpha$ take the form [88]

$$\psi_\alpha = \frac{1}{\sqrt{1 + \frac{1}{N} \sum_{j=1}^N \frac{g_c^2}{(\epsilon_\alpha - w_j)^2}}} \begin{pmatrix} \frac{g_c/\sqrt{N}}{\epsilon_\alpha - w_1} \\ \frac{g_c/\sqrt{N}}{\epsilon_\alpha - w_2} \\ \vdots \\ \frac{g_c/\sqrt{N}}{\epsilon_\alpha - w_N} \\ 1 \end{pmatrix}, \quad (\text{B3})$$

with $\alpha = \pm, 1, \dots, N - 1$. The photon weight is the squared amplitude of the $(N + 1)$ th component:

$$\text{PW}_\alpha = |\psi_{\alpha, N+1}|^2 = \frac{1}{1 + \frac{1}{N} \sum_{j=1}^N \frac{g_c^2}{(\epsilon_\alpha - w_j)^2}}. \quad (\text{B4})$$

For a dark eigenstate ψ_α ($\alpha = 1, \dots, N - 1$), the sum in the denominator is dominated by the terms where w_j is the closest to ϵ_α . Since the spacing between energies is of order $O(1/N)$, those terms are of order $O(N^2)$. With the factor $1/N$ in front of the sum, this implies that the denominator is of order $O(N)$. Thus, the photon weight of the dark states scales as

$$\text{PW}_\alpha = O(1/N). \quad (\text{B5})$$

This implies that the dark eigenstates have vanishing photon weight in the thermodynamic limit. This is in stark contrast with the photon weights of the two polariton eigenstates with energies ϵ_{\pm} , which is of order $O(1)$. Note that this argument is generally valid, beyond the perturbative limit.

The arrowhead shape of the Hamiltonian can also help to better understand the diffusion properties of the system. In particular, here we show how it can be used to argue for diffusivelike behavior of the mean-squared displacement of an excitation, $\overline{\sigma^2} \propto t$ in the strong coupling regime, and that this property originates from the contribution of dark states. We briefly sketch the argument here; a more detailed treatment will be given in Ref. [89].

In the absence of hopping and for random bare energies w_i , there is no correlation between the position of the emitters and their energy. Therefore, the probability that an excitation at emitter a arrives at emitter b at time t depends only on their bare energies w_a and w_b , but not on the distance between them (the dimensionality is also irrelevant). Then, upon averaging over disorder, all pairs of indices (a, b) with $a \neq b$ contribute the same amount to the mean-squared displacement. Therefore, the mean-squared displacement $\overline{\sigma^2}$ is proportional to the quantity

$$\overline{Q(t)} = \frac{1}{N} \sum_{1 \leq a \neq b \leq N} \overline{|e^{-i\hat{H}t}|_{ab}|^2}, \quad (\text{B6})$$

where $[e^{-i\hat{H}t}]_{ab}$ is the (a, b) entry of the $(N+1) \times (N+1)$ matrix $e^{-i\hat{H}t}$. $\overline{Q(t)}$ measures the probability that the excitation has moved at time t , regardless of its initial position. Using the fact that the matrix $e^{-i\hat{H}t}$ is unitary, one can rewrite the above sum as

$$\begin{aligned} \overline{Q(t)} &= \frac{1}{N} \sum_{a=1}^N (1 - \overline{P_{aa}(t)}) + \frac{1}{N} (1 - \overline{|[e^{-i\hat{H}t}]_{N+1, N+1}|^2}) \\ &\quad - \frac{2}{N} \sum_{a=1}^N \overline{|[e^{-i\hat{H}t}]_{a, N+1}|^2}, \end{aligned} \quad (\text{B7})$$

where $P_{aa}(t) = |[e^{-i\hat{H}t}]_{aa}|^2$ is the return probability of an excitation initially located on the emitter a . The second and third terms in Eq. (B7) remain bounded as time increases, while the first term keeps increasing and quickly becomes dominant:

$$\overline{Q(t)} \simeq \frac{1}{N} \sum_{a=1}^N (1 - \overline{P_{aa}(t)}). \quad (\text{B8})$$

The time-dependent escape probability, $(1 - \overline{P_{aa}(t)})$, thus determines the evolution of the mean-squared displacement. For large N , we can compute the evolution in the dark-state energy range in time-dependent perturbation theory and treat the evolution after initializing the system with an excitation on a single site i by using Fermi's golden rule (as shown in the next Appendix Sec. C). Then, $(1 - \overline{P_{aa}(t)}) = \Gamma_a t$, with a rate Γ_a given by Eq. (C4). This gives the linear growth:

$$\overline{\sigma^2} \propto \overline{Q(t)} \simeq \left(\frac{1}{N} \sum_{a=1}^N \Gamma_a \right) t. \quad (\text{B9})$$

In contrast, the two polaritonic states lead to $\overline{\sigma^2} \sim t^4$ at short times ($t \lesssim 1/g_c$) and generate small oscillations that are superimposed with the general linear growth predicted from the dark states [90].

APPENDIX C: SCHRIEFFER-WOLFF TRANSFORMATION AND FERMI'S GOLDEN RULE

Starting with an excitation localized on site i at time $t = 0$, we compute the escape probability $1 - P_{ii}(t)$ to other sites $j \neq i$ at time t . From energy conservation, one can already expect that these processes imply $w_i = w_j$, and therefore the perturbative expansion Eq. (A1) does not appear to be well suited as the third term on the right-hand side diverges. It is instead convenient to use a Schrieffer-Wolff transformation for the Hamiltonian $\hat{H} = \hat{H}_0 + \hat{H}_1$, which results in a disentanglement of light and matter degrees of freedom [82]. The new Hamiltonian is written as $\hat{H}' = e^{\hat{S}} \hat{H} e^{-\hat{S}}$. Under the assumption that the eigenvalues of the generator \hat{S} remain small (see below), one can expand \hat{H}' as $\hat{H}' = \hat{H} + [\hat{S}, \hat{H}] + \frac{1}{2}[\hat{S}, [\hat{S}, \hat{H}]] + \dots$. The linear coupling term \hat{H}_1 can be removed from the expansion with the choice

$$\hat{S} = \sum_i \frac{g}{w_i + \delta} (\hat{a} \hat{\sigma}_i^+ - \hat{\sigma}_i^- \hat{a}^\dagger), \quad (\text{C1})$$

which provides $[\hat{S}, \hat{H}_0] = -\hat{H}_1$. The new effective Hamiltonian (for $J = 0$) then takes the form

$$\hat{H}' = \hat{H}_0 + \frac{1}{2}[\hat{S}, \hat{H}_1] + \mathcal{O}(\hat{H}_1^3), \quad (\text{C2})$$

and the condition to be satisfied if one is to keep only the first two terms on the right-hand side of Eq. (C2) is $g \ll |w_i + \delta|$. Calculating the commutator $[\hat{S}, \hat{H}_1]$, we obtain

$$\begin{aligned} \hat{H}' &= \omega_c \hat{a}^\dagger \hat{a} + \sum_i (\omega_e + w_i) \hat{\sigma}_i^+ \hat{\sigma}_i^- + \hat{a}^\dagger \hat{a} \sum_i \frac{4g^2}{w_i + \delta} \hat{\sigma}_i^+ \hat{\sigma}_i^- \\ &\quad + \frac{g^2}{2} \sum_{i,j} \left(\frac{1}{w_i + \delta} + \frac{1}{w_j + \delta} \right) \hat{\sigma}_i^+ \hat{\sigma}_j^- \end{aligned} \quad (\text{C3})$$

up to a constant term. The last term corresponds to an effective correlated hopping between arbitrarily distant sites, while the third term results in a renormalization of the cavity frequency depending on the two-level emitter states. This term does not contribute to transitions between states with one excited emitter and zero photon, and can therefore be dropped out of the calculation. Because of the absence of divergence for $w_i = w_j$, the Hamiltonian Eq. (C3) is well suited to compute the escape probability from site i using Fermi's golden rule. The latter reads $1 - P_{ii}(t) = \Gamma_i t$, where the escape rate is (for constant $\rho(\omega) = N/W$)

$$\begin{aligned} \Gamma_i &= 2\pi \int_{-W/2}^{W/2} d\omega \rho(\omega) |\langle j, 0 | \hat{V} | i, 0 \rangle|^2 \delta(\omega - w_i) \\ &= \frac{2\pi g_c^4}{NW (w_i + \delta)^2}. \end{aligned} \quad (\text{C4})$$

Here, \hat{V} corresponds to the second term in Eq. (C3) with matrix elements (written as function of the continuous variable ω)

$$\langle j, 0 | \hat{V} | i, 0 \rangle = \frac{g^2}{2} \left(\frac{1}{w_i + \delta} + \frac{1}{\omega + \delta} \right). \quad (\text{C5})$$

Note that the two conditions $1/W \ll t \ll N/W$ and $1 - P_{ii}(t) \ll 1$ ensuring validity of Fermi's golden rule can be satisfied simultaneously in the thermodynamic limit $N \rightarrow \infty$. A lower bound for the (normalized) mean squared displacement can be estimated from Eq. (C4):

$$\frac{\overline{\sigma^2}}{N} = \frac{1}{N} \sum_{i,j} \frac{|i-j|^2}{N^2} \times \frac{1}{N} \sum_i \Gamma_i t \geq \frac{\pi g_c^4 t}{3W(W/2 + |\delta|)^2}. \quad (\text{C6})$$

This Fermi's golden rule result overestimates the numerical data plotted in Fig. 4(b) of the main text. However, those numerical results can be alternatively well described analytically using an exact formula derived directly from Eq. (B7) [89].

APPENDIX D: RETURN PROBABILITY IN 1D

In Fig. 2(a) of the main paper, we observed the appearance of the semilocalized regime by the presence of a plateau in the return probability, which is independent of N . Here, we verify that this physics is indeed independent on the dimensionality, see Fig. 5.

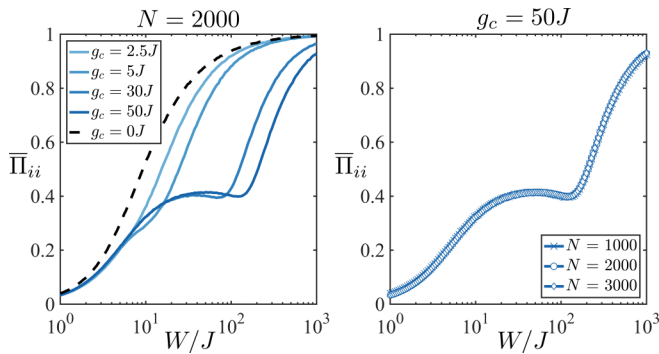


FIG. 5. (a) Disorder-averaged return probability $\bar{\Pi}_{ii}$ as a function of W/J (for a central site i of a $N = 2000$ chain, mean emitter splitting on resonance with cavity, $\delta = 0$). For strong couplings $g_c > W > W_c$, a plateau ($\bar{\Pi}_{ii} \simeq 0.4$) indicates the semilocalized regime. (b) $\bar{\Pi}_{ii}$ as a function of W/J for $g_c = 50$ and various system sizes N , demonstrating independence on N .

APPENDIX E: MODEL REALIZATION WITH COLD ATOMS

Here we discuss possible experimental implementations to observe the physics of semilocalized states with cold atoms. Such setups have been recently used to study coherent physics of the Dicke model without disorder in various scenarios.

To avoid decay of atomic excited states, it has been proposed to realize the Dicke Hamiltonian with two internal hyperfine ground states of, e.g., alkali atoms, as effective emitter states. This can be achieved by using a Raman laser dressing for atoms trapped within an optical cavity, as first suggested in Ref. [63]. Here, each atom has two long-lived ground states $|0\rangle$ and $|1\rangle$ that are coupled to the cavity mode (coupling strengths g_0 and g_1), and through a pair of balanced lasers, detuned from an excited state, with respective Rabi frequencies Ω_0 and Ω_1 (detunings Δ_0 and Δ_1). After adiabatically eliminating the atomic excited state, the two laser couplings lead effectively to resonant and counter-rotating Dicke model terms, with individually tunable Hamiltonian contributions [63]:

$$\hat{H} \propto \frac{g_0 \Omega_1}{2\Delta_1} \sum_i (\hat{a} \hat{\sigma}_i^+ + \hat{a}^\dagger \hat{\sigma}_i^-) + \frac{g_1 \Omega_0}{2\Delta_0} \sum_i (\hat{a}^\dagger \hat{\sigma}_i^+ + \hat{a} \hat{\sigma}_i^-). \quad (\text{E1})$$

To realize our Tavis-Cummings model, one can remove one laser, $\Omega_0 = 0$, see Fig. 6 for a sketch of the level scheme. This proposal has been recently experimentally realized in Ref. [64], where the two hyperfine ground states $|F = 1, m = 1\rangle \equiv |0\rangle$ and $|F = 2, m = 2\rangle \equiv |1\rangle$ of ^{87}Rb have been used. This particular experiment used a cavity with decay rate $\kappa = 2\pi \times 0.1$ MHz. Atoms are trapped in an intracavity optical lattice ensuring a location of the atoms at cavity antinodes. Such schemes allow to trap and collectively couple $\sim 10^5$ atoms [91], and can lead to effective collective coupling strengths of $g_c = \frac{g_0 \Omega_1}{2\Delta_1} \sqrt{N} \gtrsim \kappa$ overcoming the cavity decay rate. Reachable coupling strengths are simply a problem of achievable atom numbers and laser powers. Note that as an alternative to atomic ground states, long-lived excited states

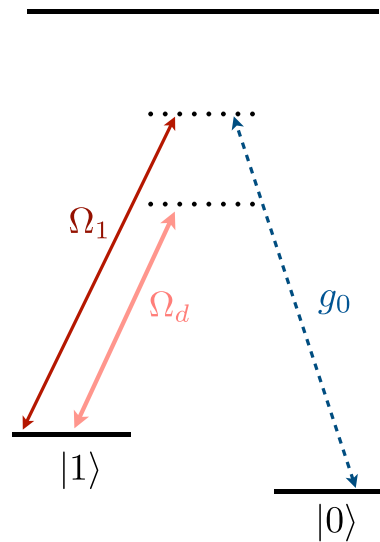


FIG. 6. Proposed level scheme for engineering the disorder Tavis-Cummings model with cold atoms. The system is based on the Raman dressing scheme from Ref. [63] that has led to experimental observation of Dicke model physics in Ref. [64].

of alkaline earth atoms may also be used. For example, in experiments as in Ref. [92], 1S_0 and 1P_1 states of Strontium atoms have been successfully used as effective emitter states to engineer infinite-range spin-models (after adiabatically eliminating the cavity).

Adding disorder to this setup can be readily achieved by superimposing additional external light fields that selectively (via the polarization) induce AC Stark shifts to one of the ground state levels (see additional disorder laser field with Rabi frequency Ω_d in Fig. 6). For example, if atoms are trapped in a regular 3D optical lattice, this can, e.g., be achieved with a second incommensurate lattice of different wavelength [59,62]. In a 1D optical lattice, random positions of atoms within “pancakes” would naturally lead to disorder. The intensity of this additional disorder light field can be sufficiently small, since the required disorder strengths for typical experimental numbers of [64,91] correspond to only $W \approx 100$ Hz $\ll g_c$ and are thus not hampering with the Raman dressing scheme. Even naturally existing disorder due to stray fields may be beneficial to study the physics described in our main text.

A cold atom setup as in Refs. [64,91] could be used for observing excitation diffusion as proposed in Fig. 4(b) in the main text, after selectively creating a population in one of the two emitter states of some atoms. Diffusion between pancakes in 1D optical lattices could be directly monitored or accessed via time-dependent measurements of emitter state populations. One could also homogeneously couple thousands of atoms with a 3D intracavity optical lattice to study diffusion on a regular lattice. This can be achieved by mode matching the lattice lasers with a cavity field as described in Ref. [93].

Finally, we remark that diffusivelike dynamics [see, e.g., Fig. 4(b) in the main text] can occur on very fast timescales, as the mean-squared displacement is proportional to the emitter number $\sigma^2 \propto N$. With experimentally achievable emitter

numbers, the diffusion rates could be made large enough such that trapping does not play a crucial role during diffusion. It may then also be practical to use (untrapped) atomic excited states as emitter states directly. Then, models with $J > 0$ can

also be considered, using atomic excitation hopping models, e.g., with Rydberg atoms as proposed in Ref. [25]. Systems using rotational states of intracavity-trapped polar molecules may also be an alternative [25].

-
- [1] M. Tavis and F. W. Cummings, Exact solution for an N -molecule-radiation-field Hamiltonian, *Phys. Rev.* **170**, 379 (1968).
- [2] H. J. Kimble, Strong interactions of single atoms and photons in cavity QED, *Phys. Scr.* **T76**, 127 (1998).
- [3] J. M. Raimond, M. Brune, and S. Haroche, Manipulating quantum entanglement with atoms and photons in a cavity, *Rev. Mod. Phys.* **73**, 565 (2001).
- [4] Y. Kaluzny, P. Goy, M. Gross, J. M. Raimond, and S. Haroche, Observation of Self-Induced Rabi Oscillations in Two-Level Atoms Excited Inside a Resonant Cavity: The Ringing Regime of Superradiance, *Phys. Rev. Lett.* **51**, 1175 (1983).
- [5] M. G. Raizen, R. J. Thompson, R. J. Brecha, H. J. Kimble, and H. J. Carmichael, Normal-Mode Splitting and Linewidth Averaging for Two-State Atoms in an Optical Cavity, *Phys. Rev. Lett.* **63**, 240 (1989).
- [6] R. J. Thompson, G. Rempe, and H. J. Kimble, Observation of Normal-Mode Splitting for an Atom in an Optical Cavity, *Phys. Rev. Lett.* **68**, 1132 (1992).
- [7] C. Weisbuch, M. Nishioka, A. Ishikawa, and Y. Arakawa, Observation of the Coupled Exciton-Photon Mode Splitting in a Semiconductor Quantum Microcavity, *Phys. Rev. Lett.* **69**, 3314 (1992).
- [8] A. Imamoğlu, R. J. Ram, S. Pau, and Y. Yamamoto, Nonequilibrium condensates and lasers without inversion: Exciton-polariton lasers, *Phys. Rev. A* **53**, 4250 (1996).
- [9] D. G. Lidzey, D. D. C. Bradley, M. S. Skolnick, T. Virgili, S. Walker, and D. M. Whittaker, Strong exciton-photon coupling in an organic semiconductor microcavity, *Nature* **395**, 53 (1998).
- [10] J. M. Fink, R. Bianchetti, M. Baur, M. Göppl, L. Steffen, S. Filipp, P. J. Leek, A. Blais, and A. Wallraff, Dressed Collective Qubit States and the Tavis-Cummings Model in Circuit QED, *Phys. Rev. Lett.* **103**, 083601 (2009).
- [11] Y. Kubo, F. R. Ong, P. Bertet, D. Vion, V. Jacques, D. Zheng, A. Dréau, J.-F. Roch, A. Auffeves, F. Jelezko, J. Wrachtrup, M. F. Barthe, P. Bergonzo, and D. Esteve, Strong Coupling of a Spin Ensemble to a Superconducting Resonator, *Phys. Rev. Lett.* **105**, 140502 (2010).
- [12] Y. Tabuchi, S. Ishino, T. Ishikawa, R. Yamazaki, K. Usami, and Y. Nakamura, Hybridizing Ferromagnetic Magnons and Microwave Photons in the Quantum Limit, *Phys. Rev. Lett.* **113**, 083603 (2014).
- [13] M. A. Sentef, M. Ruggenthaler, and A. Rubio, Cavity quantum-electrodynamical polaritonically enhanced electron-phonon coupling and its influence on superconductivity, *Sci. Adv.* **4**, eaau6969 (2018).
- [14] A. Thomas, E. Devaux, K. Nagarajan, T. Chervy, M. Seidel, D. Hagenmüller, S. Schütz, J. Schachenmayer, C. Genet, G. Pupillo, and T. W. Ebbesen, Exploring superconductivity under strong coupling with the vacuum electromagnetic field, [arXiv:1911.01459](https://arxiv.org/abs/1911.01459).
- [15] A. Thomas, L. Lethuillier-Karl, K. Nagarajan, R. M. A. Vergauwe, J. George, T. Chervy, A. Shalabney, E. Devaux, C. Genet, J. Moran, and T. W. Ebbesen, Tilting a ground-state reactivity landscape by vibrational strong coupling, *Science* **363**, 615 (2019).
- [16] S. Kéna-Cohen and J. Yuen-Zhou, Polariton chemistry: Action in the dark, *ACS Cent. Sci.* **5**, 386 (2019).
- [17] J. Lather, P. Bhatt, A. Thomas, T. W. Ebbesen, and J. George, Cavity catalysis by cooperative vibrational strong coupling of reactant and solvent molecules, *Angew. Chem. Int. Ed.* **58**, 10635 (2019).
- [18] A. Thomas, J. George, A. Shalabney, M. Dryzhakov, S. J. Varma, J. Moran, T. Chervy, X. Zhong, E. Devaux, C. Genet, J. A. Hutchison, and T. W. Ebbesen, Ground-state chemical reactivity under vibrational coupling to the vacuum electromagnetic field, *Angew. Chem. Int. Ed.* **55**, 11462 (2016).
- [19] J. A. Hutchison, T. Schwartz, C. Genet, E. Devaux, and T. W. Ebbesen, Modifying chemical landscapes by coupling to vacuum fields, *Angew. Chem. Int. Ed.* **51**, 1592 (2012).
- [20] F. Herrera and F. C. Spano, Cavity-Controlled Chemistry in Molecular Ensembles, *Phys. Rev. Lett.* **116**, 238301 (2016).
- [21] J. Galego, F. J. Garcia-Vidal, and J. Feist, Suppressing photochemical reactions with quantized light fields, *Nat. Commun.* **7**, 13841 (2016).
- [22] J. Flick, M. Ruggenthaler, H. Appel, and A. Rubio, Atoms and molecules in cavities, from weak to strong coupling in quantum-electrodynamics (QED) chemistry, *Proc. Natl. Acad. Sci. USA* **114**, 3026 (2017).
- [23] D. M. Coles, N. Somaschi, P. Michetti, C. Clark, P. G. Lagoudakis, P. G. Savvidis, and D. G. Lidzey, Polariton-mediated energy transfer between organic dyes in a strongly coupled optical microcavity, *Nat. Mater.* **13**, 712 (2014).
- [24] J. Feist and F. J. Garcia-Vidal, Extraordinary Exciton Conductance Induced by Strong Coupling, *Phys. Rev. Lett.* **114**, 196402 (2015).
- [25] J. Schachenmayer, C. Genes, E. Tignone, and G. Pupillo, Cavity-Enhanced Transport of Excitons, *Phys. Rev. Lett.* **114**, 196403 (2015).
- [26] X. Zhong, T. Chervy, L. Zhang, A. Thomas, J. George, C. Genet, J. A. Hutchison, and T. W. Ebbesen, Energy transfer between spatially separated entangled molecules, *Angew. Chem. Int. Ed.* **56**, 9034 (2017).
- [27] G. Lerario, D. Ballarini, A. Fieramosca, A. Cannavale, A. Genco, F. Mangione, S. Gambino, L. Dominici, M. De Giorgi, G. Gigli, and D. Sanvitto, High-speed flow of interacting organic polaritons, *Light: Sci. Appl.* **6**, e16212 (2017).
- [28] M. Reitz, F. Mineo, and C. Genes, Energy transfer and correlations in cavity-embedded donor-acceptor configurations, *Sci. Rep.* **8**, 1 (2018).

- [29] M. Du, L. A. Martínez-Martínez, R. F. Ribeiro, Z. Hu, V. M. Menon, and J. Yuen-Zhou, Theory for polariton-assisted remote energy transfer, *Chem. Sci.* **9**, 6659 (2018).
- [30] C. Schäfer, M. Ruggenthaler, H. Appel, and A. Rubio, Modification of excitation and charge transfer in cavity quantum-electrodynamical chemistry, *Proc. Natl. Acad. Sci. USA* **116**, 4883 (2019).
- [31] E. Orgiu, J. George, J. A. Hutchison, E. Devaux, J. F. Dayen, B. Doudin, F. Stellacci, C. Genet, J. Schachenmayer, C. Genes, G. Pupillo, P. Samorì, and T. W. Ebbesen, Conductivity in organic semiconductors hybridized with the vacuum field, *Nat. Mater.* **14**, 1123 (2015).
- [32] D. Hagenmüller, J. Schachenmayer, S. Schütz, C. Genes, and G. Pupillo, Cavity-Enhanced Transport of Charge, *Phys. Rev. Lett.* **119**, 223601 (2017).
- [33] D. Hagenmüller, S. Schütz, J. Schachenmayer, C. Genes, and G. Pupillo, Cavity-assisted mesoscopic transport of fermions: Coherent and dissipative dynamics, *Phys. Rev. B* **97**, 205303 (2018).
- [34] F. Evers and A. D. Mirlin, Anderson transitions, *Rev. Mod. Phys.* **80**, 1355 (2008).
- [35] P. W. Anderson, Absence of diffusion in certain random lattices, *Phys. Rev.* **109**, 1492 (1958).
- [36] E. Abrahams, P. W. Anderson, D. C. Licciardello, and T. V. Ramakrishnan, Scaling Theory of Localization: Absence of Quantum Diffusion in two Dimensions, *Phys. Rev. Lett.* **42**, 673 (1979).
- [37] R. Houdré, R. P. Stanley, and M. Ilegems, Vacuum-field Rabi splitting in the presence of inhomogeneous broadening: Resolution of a homogeneous linewidth in an inhomogeneously broadened system, *Phys. Rev. A* **53**, 2711 (1996).
- [38] P. R. Eastham and P. B. Littlewood, Bose condensation of cavity polaritons beyond the linear regime: The thermal equilibrium of a model microcavity, *Phys. Rev. B* **64**, 235101 (2001).
- [39] M. Litinskaia, G. C. La Rocca, and V. M. Agranovich, Inhomogeneous broadening of polaritons in high-quality microcavities and weak localization, *Phys. Rev. B* **64**, 165316 (2001).
- [40] F. M. Marchetti, J. Keeling, M. H. Szymańska, and P. B. Littlewood, Thermodynamics and Excitations of Condensed Polaritons in Disordered Microcavities, *Phys. Rev. Lett.* **96**, 066405 (2006).
- [41] F. M. Marchetti, J. Keeling, M. H. Szymańska, and P. B. Littlewood, Absorption, photoluminescence, and resonant Rayleigh scattering probes of condensed microcavity polaritons, *Phys. Rev. B* **76**, 115326 (2007).
- [42] P. Kirton, M. M. Roses, J. Keeling, and E. G. D. Torre, Introduction to the Dicke model: From equilibrium to nonequilibrium, and vice versa, *Adv. Quantum Technol.* **2**, 1800043 (2019).
- [43] C. Gonzalez-Ballester, J. Feist, E. Gonzalo Badía, E. Moreno, and F. J. Garcia-Vidal, Uncoupled Dark States can Inherit Polaritonic Properties, *Phys. Rev. Lett.* **117**, 156402 (2016).
- [44] I. Carusotto and C. Ciuti, Quantum fluids of light, *Rev. Mod. Phys.* **85**, 299 (2013).
- [45] P. Törmä and W. L. Barnes, Strong coupling between surface plasmon polaritons and emitters: a review, *Rep. Prog. Phys.* **78**, 013901 (2014).
- [46] D. Sanvitto and S. Kéna-Cohen, The road towards polaritonic devices, *Nat. Mater.* **15**, 1061 (2016).
- [47] S. Putz, A. Angerer, D. O. Krimer, R. Glattauer, W. J. Munro, S. Rotter, J. Schmiedmayer, and J. Majer, Spectral hole burning and its application in microwave photonics, *Nat. Photonics* **11**, 36 (2016).
- [48] H. Deng, G. Weihs, C. Santori, J. Bloch, and Y. Yamamoto, Condensation of semiconductor microcavity exciton polaritons, *Science* **298**, 199 (2002).
- [49] J. Kasprzak, M. Richard, S. Kundermann, A. Baas, P. Jeambrun, J. M. J. Keeling, F. M. Marchetti, M. H. Szymańska, R. André, J. L. Staehli, V. Savona, P. B. Littlewood, B. Deveaud, and L. S. Dang, Bose–Einstein condensation of exciton polaritons, *Nature* **443**, 409 (2006).
- [50] R. Balili, V. Hartwell, D. Snoke, L. Pfeiffer, and K. West, Bose–Einstein condensation of microcavity polaritons in a trap, *Science* **316**, 1007 (2007).
- [51] A. Amo, D. Sanvitto, F. P. Laussy, D. Ballarini, E. d. Valle, M. D. Martin, A. Lemaître, J. Bloch, D. N. Krizhanovskii, M. S. Skolnick, C. Tejedor, and L. Viña, Collective fluid dynamics of a polariton condensate in a semiconductor microcavity, *Nature* **457**, 291 (2009).
- [52] A. Amo, J. Lefrère, S. Pigeon, C. Adrados, C. Ciuti, I. Carusotto, R. Houdré, E. Giacobino, and A. Bramati, Superfluidity of polaritons in semiconductor microcavities, *Nat. Phys.* **5**, 805 (2009).
- [53] J. Keeling, M. J. Bhaseen, and B. D. Simons, Collective Dynamics of Bose-Einstein Condensates in Optical Cavities, *Phys. Rev. Lett.* **105**, 043001 (2010).
- [54] H. Deng, H. Haug, and Y. Yamamoto, Exciton-polariton Bose-Einstein condensation, *Rev. Mod. Phys.* **82**, 1489 (2010).
- [55] R. T. Juggins, J. Keeling, and M. H. Szymańska, Coherently driven microcavity-polaritons and the question of superfluidity, *Nat. Commun.* **9**, 4062 (2018).
- [56] F. Cadiz, C. Robert, E. Courtade, M. Manca, L. Martinelli, T. Taniguchi, K. Watanabe, T. Amand, A. C. H. Rowe, D. Paget, B. Urbaszek, and X. Marie, Exciton diffusion in WSe₂ monolayers embedded in a Van der Waals heterostructure, *Appl. Phys. Lett.* **112**, 152106 (2018).
- [57] S. S. Wang, X. J. Li, W. L. Zhang, and C. Y. Zheng, Transverse Anderson localization of exciton-polaritons in microcavities with single-layer WS₂, *IEEE J. Sel. Top. Quantum Electron.* **25**, 1 (2019).
- [58] J. Billy, V. Josse, Z. Zuo, A. Bernard, B. Hambrecht, P. Lugan, D. Clément, L. Sanchez-Palencia, P. Bouyer, and A. Aspect, Direct observation of Anderson localization of matter waves in a controlled disorder, *Nature* **453**, 891 (2008).
- [59] G. Roati, C. D’Errico, L. Fallani, M. Fattori, C. Fort, M. Zaccanti, G. Modugno, M. Modugno, and M. Inguscio, Anderson localization of a non-interacting Bose–Einstein condensate, *Nature* **453**, 895 (2008).
- [60] S. S. Kondov, W. R. McGehee, J. J. Zirbel, and B. DeMarco, Three-dimensional Anderson localization of ultracold matter, *Science* **334**, 66 (2011).
- [61] F. Jendrzejewski, A. Bernard, K. Müller, P. Cheinet, V. Josse, M. Piraud, L. Pezzé, L. Sanchez-Palencia, A. Aspect, and P. Bouyer, Three-dimensional localization of ultracold atoms in an optical disordered potential, *Nat. Phys.* **8**, 398 (2012).
- [62] M. Schreiber, S. S. Hodgman, P. Bordia, H. P. Lüschen, M. H. Fischer, R. Vosk, E. Altman, U. Schneider, and I. Bloch, Observation of many-body localization of interacting fermions in a quasirandom optical lattice, *Science* **349**, 842 (2015).
- [63] F. Dimer, B. Estienne, A. S. Parkins, and H. J. Carmichael, Proposed realization of the Dicke-model quantum phase

- transition in an optical cavity QED system, *Phys. Rev. A* **75**, 013804 (2007).
- [64] Z. Zhang, C. H. Lee, R. Kumar, K. J. Arnold, S. J. Masson, A. L. Grimsmo, A. S. Parkins, and M. D. Barrett, Dicke-model simulation via cavity-assisted Raman transitions, *Phys. Rev. A* **97**, 043858 (2018).
- [65] M. Gaudin, Diagonalisation d'une classe d'hamiltoniens de spin, *J. Phys.* **37**, 1087 (1976).
- [66] J. Dukelsky, S. Pittel, and G. Sierra, Colloquium: Exactly solvable Richardson-Gaudin models for many-body quantum systems, *Rev. Mod. Phys.* **76**, 643 (2004).
- [67] J. Schliemann, A. Khaetskii, and D. Loss, Electron spin dynamics in quantum dots and related nanostructures due to hyperfine interaction with nuclei, *J. Phys.: Condens. Matter* **15**, R1809 (2003).
- [68] M. Bortz and J. Stolze, Exact dynamics in the inhomogeneous central-spin model, *Phys. Rev. B* **76**, 014304 (2007).
- [69] A. Faribault and D. Schuricht, Integrability-Based Analysis of the Hyperfine-Interaction-Induced Decoherence in Quantum Dots, *Phys. Rev. Lett.* **110**, 040405 (2013).
- [70] D. Hetterich, M. Serbyn, F. Domínguez, F. Pollmann, and B. Trauzettel, Noninteracting central site model: Localization and logarithmic entanglement growth, *Phys. Rev. B* **96**, 104203 (2017).
- [71] D. Hetterich, N. Y. Yao, M. Serbyn, F. Pollmann, and B. Trauzettel, Detection and characterization of many-body localization in central spin models, *Phys. Rev. B* **98**, 161122(R) (2018).
- [72] M. O. Scully and M. S. Zubairy, *Quantum Optics* (Cambridge University Press, Cambridge, UK, 1997).
- [73] A. MacKinnon and B. Kramer, One-Parameter Scaling of Localization Length and Conductance in Disordered Systems, *Phys. Rev. Lett.* **47**, 1546 (1981).
- [74] E. Hofstetter and M. Schreiber, Finite-size scaling and critical exponents. A new approach and its application to Anderson localisation, *Europhys. Lett.* **21**, 933 (1993).
- [75] B. I. Shklovskii, B. Shapiro, B. R. Sears, P. Lambrianides, and H. B. Shore, Statistics of spectra of disordered systems near the metal-insulator transition, *Phys. Rev. B* **47**, 11487 (1993).
- [76] I. K. Zharekeshev and B. Kramer, Scaling of level statistics at the disorder-induced metal-insulator transition, *Phys. Rev. B* **51**, 17239 (1995).
- [77] G. Celardo, A. Biella, L. Kaplan, and F. Borgonovi, Interplay of superradiance and disorder in the Anderson Model, *Fortschr. Phys.* **61**, 250 (2013).
- [78] A. Biella, F. Borgonovi, R. Kaiser, and G. L. Celardo, Subradiant hybrid states in the open 3D Anderson-Dicke model, *EPL* **103**, 57009 (2013).
- [79] F. Haake, *Quantum Signatures of Chaos* (Springer-Verlag, Berlin, 2006).
- [80] E. B. Bogomolny, U. Gerland, and C. Schmit, Models of intermediate spectral statistics, *Phys. Rev. E* **59**, R1315 (1999).
- [81] N. C. Chávez, F. Mattiotti, J. A. Méndez-Bermúdez, F. Borgonovi, and G. L. Celardo, Disorder-Enhanced and Disorder-Independent Transport with long-range hopping: Application to molecular chains in optical cavities, [arXiv:2010.08060](https://arxiv.org/abs/2010.08060).
- [82] G. Zhu, S. Schmidt, and J. Koch, Dispersive regime of the Jaynes-Cummings and Rabi lattice, *New J. Phys.* **15**, 115002 (2013).
- [83] L. S. Levitov, Delocalization of Vibrational Modes Caused by Electric Dipole Interaction, *Phys. Rev. Lett.* **64**, 547 (1990).
- [84] A. D. Mirlin, Y. V. Fyodorov, F.-M. Dittes, J. Quezada, and T. H. Seligman, Transition from localized to extended eigenstates in the ensemble of power-law random banded matrices, *Phys. Rev. E* **54**, 3221 (1996).
- [85] G. L. Celardo, R. Kaiser, and F. Borgonovi, Shielding and localization in the presence of long-range hopping, *Phys. Rev. B* **94**, 144206 (2016).
- [86] X. Deng, B. L. Altshuler, G. V. Shlyapnikov, and L. Santos, Quantum Levy Flights and Multifractality of Dipolar Excitations in a Random System, *Phys. Rev. Lett.* **117**, 020401 (2016).
- [87] X. Deng, V. E. Kravtsov, G. V. Shlyapnikov, and L. Santos, Duality in Power-Law Localization in Disordered One-Dimensional Systems, *Phys. Rev. Lett.* **120**, 110602 (2018).
- [88] D. O'Leary and G. Stewart, Computing the eigenvalues and eigenvectors of symmetric arrowhead matrices, *J. Comput. Phys.* **90**, 497 (1990).
- [89] J. Dubail, T. Botzung, D. Hagenmüller, G. Pupillo, and J. Schachenmayer (unpublished).
- [90] T. Botzung, Study of strongly correlated one-dimensional systems with long-range interactions, Ph.D. thesis, University of Strasbourg, Ecole Doctorale des Sciences Chimiques, 2019.
- [91] Z. Zhiqiang, C. H. Lee, R. Kumar, K. J. Arnold, S. J. Masson, A. S. Parkins, and M. D. Barrett, Nonequilibrium phase transition in a spin-1 Dicke model, *Optica* **4**, 424 (2017).
- [92] J. A. Muniz, D. Barberena, R. J. Lewis-Swan, D. J. Young, J. R. K. Cline, A. M. Rey, and J. K. Thompson, Exploring dynamical phase transitions with cold atoms in an optical cavity, *Nature* **580**, 602 (2020).
- [93] D. Wellnitz, S. Schütz, S. Whitlock, J. Schachenmayer, and G. Pupillo, Collective dissipative molecule formation in a cavity, *Phys. Rev. Lett.* (to be published) [[arXiv:2002.05601](https://arxiv.org/abs/2002.05601)].